Development of a deep-water carbonate ion concentration proxy based on preservation of planktonic foraminifera shells quantified by X-ray CT scanning

S. Iwasaki[1*], K. Kimoto[2], M. Kucera[1]

[1]MARUM - Center for Marine Environmental Sciences, University of Bremen, Bremen, Germany
[2] Japan Agency for Marine-Earth Science and Technology, Research Institute for Global Change, Yokosuka, Japan

Corresponding author: Shinya Iwasaki (siwasaki@marum.de)

Key Points:

- Planktonic foraminiferal shell dissolution intensity was determined by CT-based proxy using core top samples in the Southern Atlantic Ocean.
- The characteristics and reliability of CT-based proxy were assessed by comparing with conventional proxy.
- The CT-based proxy is available for reconstructing deep seawater carbonate ion concentration under the appropriate condition.

Abstract

The quantitative and objective characterization of dissolution intensity in fossil planktonic foraminiferal shells could be used to reconstruct past changes in bottom water carbonate ion concentration. Among proxies measuring the degree of dissolution of planktonic foraminiferal shells, X-ray micro-Computed Tomography (CT) based characterization of apparent shell density appears to have good potential to facilitate quantitative reconstruction of carbonate chemistry. However, unlike the well-established benthic foraminiferal B/Ca ratio-based proxy, only a regional calibration of the CT-based proxy exists based on a limited number of data points covering mainly low-saturation state waters. Here we determined by CT-based proxy the shell dissolution intensity of planktonic foraminifera *Globigerina bulloides, Globorotalia inflata, Globigerinoides ruber*, and *Trilobatus sacculifer* from a collection of core top samples in the Southern Atlantic covering higher saturation states, and assessed the characteristics and reliability of CT-based proxy. We observed that the CT-based proxy is generally controlled by deep-water $\Delta[CO_3^{2-}]$ like the B/Ca proxy, but its effective range of $\Delta[CO_3^{2-}]$ is between –20 to 10 $\mu molkg^{-1}$. In this range, the CT-based proxy appears directly and strongly related to deep-water $\Delta[CO_3^{2-}]$, whereas the B/Ca of benthic foraminifera appears to be affected by porewater saturation in carbonate-rich substrates. On the other hand, the CT-based proxy is affected by supralysoclinal dissolution in areas with high productivity. Like the B/Ca proxy, the CT-based proxy requires species-specific calibration, but the effect of species-specific shell difference in susceptibility to dissolution on the proxy is small.

1 Introduction

The atmospheric CO_2 concentration has fluctuated by ~80 ppm between glacial and interglacial periods, implying a large and rapid exchange of carbon between the atmosphere and the ocean on those time scales [Barnola et al., 1987; Petit et al., 1999]. This is because the oceanic carbon pool is about 50 times larger than that of the atmosphere [Sigman and Boyle, 2000], and carbon storage in the deep ocean and changes in deep-water circulation can substantially alter atmospheric pCO_2. However, data concerning the amount of carbon storage in the deep sea and their temporal and spatial variation, which are essential to understand the glacial-interglacial pCO_2 exchange between ocean and atmosphere, is insufficient. Because the deep seawater carbonate ion concentration ($[CO_3^{2-}]$) is governed primarily by the concentration of dissolved inorganic carbon and alkalinity, its reconstruction can provide valuable insights into the changes in the global carbon cycle.

The B/Ca ratio of epifaunal benthic foraminifera has been proposed as a quantitative deep seawater $[CO_3^{2-}]$ proxy [e.g., Yu and Elderfield, 2007]. This proxy relies on the fact that the ratio of the two major boron species in the deep seawater, $B(OH)_3$ and $B(OH)_4^-$, varies with pH [Hemming et al., 1992] and these variations are reflected in the B/Ca ratio in shell calcite. Indeed, a significant correlation between B/Ca ratio in the shells of *Cibicidoides wuellerstorfi* and deep seawater $\Delta[CO_3^{2-}]$ was shown by Yu and Elderfield [2007]. The sensitivity of *C. wuellerstorfi* B/Ca ratio to deep seawater $\Delta[CO_3^{2-}]$ was evaluated based on core-top calibration at more than 200 sites, indicating an uncertainty of ±5 $\mu mol\ kg^{-1}$ in $[CO_3^{2-}]$ (Brown and Elderfield, 1996, Rae et al., 2011, Raitzsch et al., 2011, Yu and Elderfield., 2007, Yu et al., 2013, 2014, Brown et al., 2011). Based on this calibration, subsequent studies reconstructed temporal variations in deep seawater $[CO_3^{2-}]$ at several sites, where the sediment samples contain

sufficient amount of benthic foraminifera shells of the target species [e.g., Yu et al., 2016, 2020, Allen et al., 2015, 2019]. Next to the most frequently used calibration based on *C. wuellerstorfi*, there also exist data for another epifaunal species, *C. mundulus*, confirming a relationship between shell B/Ca and deep seawater $\Delta[CO_3^{2-}]$, but the calibration shows a different slope, indicating that the incorporation of B into the shell calcite is affected by species-specific processes. Therefore, the B/Ca method can only be applied where the same species occurs throughout the studied interval and also where a sufficient number of shells can be recovered to facilitate the chemical analysis. This prevents applications in settings where the regional environmental change caused large shifts in food availability and bottom water oxygen content, resulting in shifts in benthic communities, as well as in settings with high sedimentation rate, where the concentration of foraminifera shells is low (e.g. Kitazato et al., 2000, Gooday, 2003, Geslin et al., 2004).

Planktonic foraminifera shells are a primary component of carbonate in the deep-sea sediment (Schiebel, 2002), and the preservation of these shells is intimately associated with the deep seawater $\Delta[CO_3^{2-}]$ (e.g., Berger et al., 1982). Therefore, another way to reconstruct deep seawater $[CO_3^{2-}]$ is by the quantification of the degree of dissolution of planktonic foraminifera shells (e.g. Berger et al., 1982). Previous studies made use of this relationship, but applied different ways to quantify dissolution intensity, such as by shell fragmentation, proportion of dissolution resistant species or the ratio between benthic and planktonic foraminifera (Berger et al., 1982, Peterson and Prell, 1985, Kucera, 2007). These proxies all show the expected direction of the relationship with deep seawater $\Delta[CO_3^{2-}]$, but are either hard to objectively quantify or are affected by initial conditions (assemblage composition) (Kucera, 2007). The size-normalized weight of sedimentary shell was proposed to quantify carbonate dissolution intensity more objectively (Lohmann, 1995, Broecker and Clark, 2001). However, the initial weight of the planktonic foraminifera shell is also controlled by surface water properties, such as surface water carbonate chemistry (e.g., Barker and Elderfield, 2002; Marshall et al., 2013) making quantitative reconstructions of deep-water $[CO_3^{2-}]$ impossible in settings where surface properties have changed as well.

More recent studies suggested that the problem of quantifying preservation state of planktonic foraminifera shells can be circumvented by measurements of shell architecture using X-ray micro-CT scanning (Johnstone et al., 2010, Iwasaki et al., 2015, Iwasaki et al., 2019). In particular, the quantification of shell preservation by measuring the proportion of more strongly dissolved calcite, identified by their lower CT number, provides a means to objectively determine the preservation state in a way that is not dependent on the initial size or weight of the shell. As long as the ratio of the different types of calcites, making up the lamellar structure of the shells remains the same, the proportion of the more dissolved calcite should only be related to deep-water $[CO_3^{2-}]$ (Iwasaki et al., 2015, Iwasaki et al., 2019). However, so far only a regional South pacific calibration of the CT-based proxy exists (Iwasaki et al., 2022). This calibration is based on a limited number of data points, covering mainly low saturation state waters, and it has not been directly compared with the B/Ca proxy.

In addition, there are factors other than deep seawater $[CO_3^{2-}]$ variation that control carbonate dissolution on the deep seafloor and which may affect the CT-based proxy differently than the B/Ca proxy. The first factor is the variation in sedimentation rate, which alters the exposure time to deep seawater and results in differences in dissolution intensity of planktonic foraminifera shells (Berger et al., 1982). The second factor is the decomposition of organic material in the sediment, which decreases ambient seawater (or porewater) $[CO_3^{2-}]$ and may

cause carbonate dissolution in seafloor sediments deposited above the regional lysocline (Berger et al., 1970, Milliman, 1993, Hales and Emerson, 1996, Hales, 2003). Finally, it is known from earlier attempts to use the preservation of planktonic foraminifera shells as a proxy for deep-water properties that significant changes in preservation are only encountered below a certain critical threshold value of deep seawater [CO_3^{2-}], and shells deposited above this foraminiferal lysocline all appear well preserved (Berger et al., 1982). Therefore, to develop the method using CT-scanning of planktonic foraminiferal shells as paleo-deep seawater [CO_3^{2-}] proxy, assessing the effect of these secondary factors on the preservation state of shells deposited in various sedimentary settings is necessary.

To assess the accuracy and reliability of the CT-based proxy for deep seawater [CO_3^{2-}] reconstruction, we have quantified planktonic foraminifera shell preservation in a collection of samples from the South Atlantic, covering a gradient towards higher ambient $\Delta[CO_3^{2-}]$ values, and representing different sedimentation rates and productivity regimes. Importantly, in all the analyzed samples, B/Ca of *C. wuellerstorfi* have been determined by (Rae et al., 2011, Raitzsch et al., 2013), allowing direct proxy intercomparison. We quantified the degree of shell dissolution in four planktonic foraminifera species (*G. bulloides*, *G. inflata, G. ruber,* and *T. sacculifer*) and propose a new way to quantify the proportion of more dissolved calcite, which does not require instrument-specific calibration of the strength of the X-ray beam. We combine the new measurements with previously obtained CT images (Iwasaki et al., 2019, 2022) to determine the regional and species-specific effects and establish a new calibration formula, allowing reconstructions of deep seawater $\Delta[CO_3^{2-}]$.

2 Materials and Methods

2.1. Multiple core samples and physicochemical properties

In this study, we used planktonic foraminifera shells extracted from 13 core top samples collected by multiple corer between 940 and 4173 m water depth in the South Atlantic (Figure 1). The samples represent a subset of core tops where benthic foraminiferal (*Cibicidoides wuellerstorfi*) B/Ca ratio, a conventional proxy of deep seawater [CO_3^{2-}], has been determined by previous studies (Rae et al., 2011, Raitzsch et al., 2013) (Figure 2). The subset contains all samples used in the previous studies for which the material is stored in the GeoB repository in Bremen and where information is available on sedimentation rate and accumulation rate of organic carbon. From each core top sample, eight shells of each of four planktic foraminiferal species (*G. bulloides*, *G. inflata, G. ruber,* and *T. sacculifer*) were collected for analysis by X-ray micro-CT scanning. Among the 13 sites, shells of *G. bulloides* could be collected from all sites, shells of *G. inflata* and *T. sacculifer* were collected from 12 sites, and shells of *G. ruber* were collected from 11 sites. The all shells were collected from the 300-355 µm size fraction, and are not fragmented or containing fractures and holes, or peeling of the surface. Estimates of sedimentation rate (cm kyr^{-1}) at the studied sites were taken from age models of sediment cores sampled at the same site (Wefer et al., 1990, Schulz et al., 1992, 1996; Bleil et al. 2001), and used to calculate accumulation rate of organic carbon (g cm^{-2} kyr^{-1}) making use of total organic carbon content (%TOC) and dry bulk density (g cm–3) data for each site (Mollenhauer et al., 2004).

In addition to the above sample set, we used a subset of published 16 core top samples from the Pacific Ocean to extend the dissolution intensity calibration over a larger range of deep

seawater $\Delta[CO_3^{2-}]$ values (Iwasaki et al., 2019, 2022). The core top sediment samples were obtained by multiple core sampling from the water depth between 1500 and 4000 m, with most of them located below the dissolution transition depth level ($\Delta[CO_3^{2-}]$ < 10 µmol kg^{-1}). From each core top sample, more than eight shells of each of three planktic foraminiferal species (*G. bulloides*, *G. ruber,* and *T. sacculifer*) without external damage were collected from 200-355 µm size fraction for analysis by X-ray micro-CT scanning in previous studies, and the existing scans were here used for the calculation of the newly defined CT based dissolution index (Iwasaki et al., 2019 and 2022). To remain consistent with the existing data and due to the difficulty to unambiguously and consistently separating both species (Morard et al., 2019), specimens designated as *G. ruber* may contain both *G. ruber albus* and *G. elongatus*.

Bottom water values of $\Delta[CO_3^{2-}]$ for the all of studied sites were calculated from physicochemical parameters (temperature, salinity, total alkalinity, total inorganic carbon, and concentrations of phosphate and silicate) measured at nearby Global Ocean Data Analysis Project (GLODAP) profiles (Key et al., 2004). The site information and the estimated values of bottom water physicochemical properties for all Atlantic and Pacific sites are summarized in Table 1.

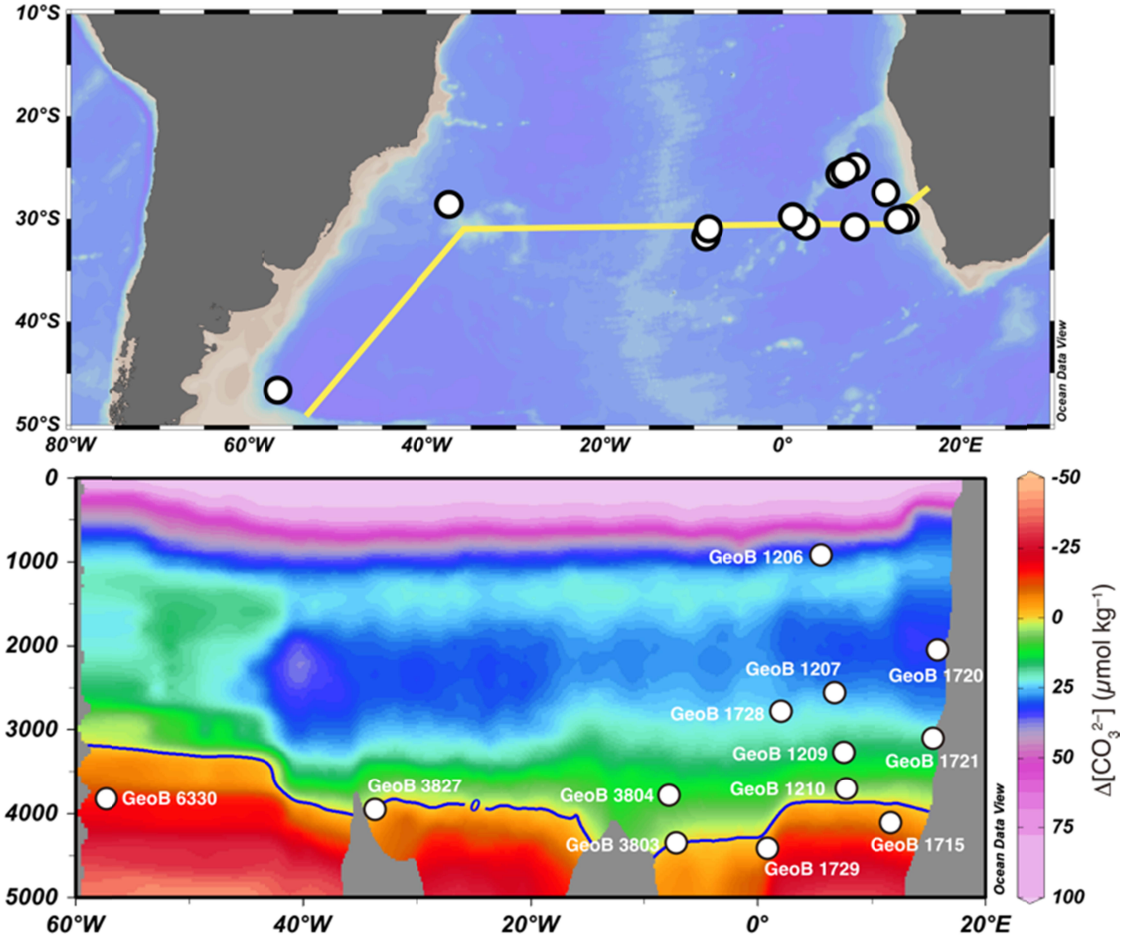

Figure 1. The locations of multiple corer samples in the South Atlantic used in this study. The section along the yellow line is showing the spatial distribution of the degree of carbonate saturation ($\Delta[CO_3^{2-}]$) in the study area.

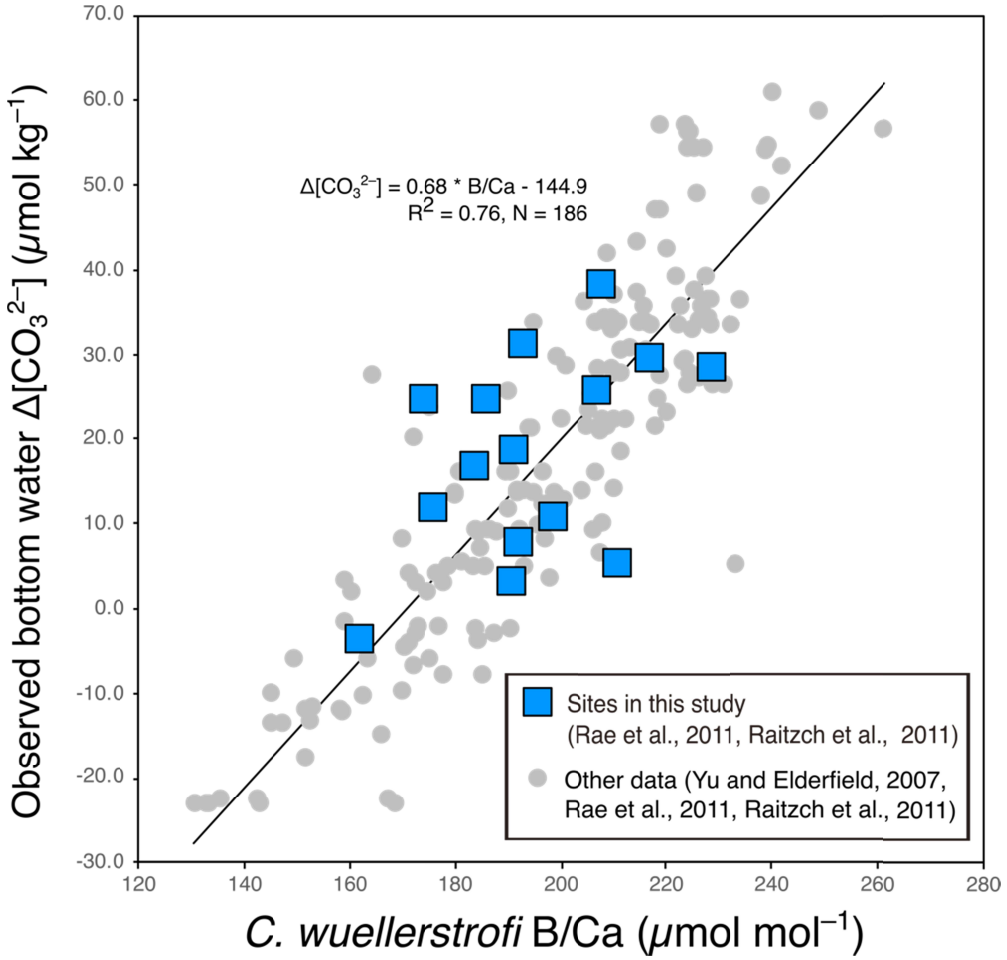

Figure 2. B/Ca ratio in shells of the benthic foraminifera *Cibicidoides wuellerstorfi* in core top samples plotted against deep-water $\Delta[CO_3^{2-}]$. The data of B/Ca ratio of benthic foraminifera in the core-top sample used in this study are shown by blue squares. Data are derived from Rae et al. (2011), Raitzch et al. (2011), and Yu and Elderfield (2007).

Cruise	Site	Latitude (S)	longitude (W)	Depth (m)	Deep water $\Delta[CO_3^{2-}]$ (μmol kg^{-1})	Linear Sedimentation Rate (cm kyr^{-1})	TOC accumulation rate (g m^{-2} y^{-1})	Caronate content (%)	C. w_B/Ca (μmol mol^{-1})	error
M 12/1	1206-1	24.67	-6.48	940	25.1	No data	No data	No data	193	4
M 12/1	1207-2	24.59	-6.85	2593	29.9	1.5	0.17	95.5	217	7
M 12/1	1209-1	24.50	-7.28	3303	14.6	3.3	0.41	95.9	191	9
M 12/1	1210-3	24.48	-7.43	3750	6.5	1.4	0.16	93.7	192	5
M 20/2	1715-1	26.47	-11.63	4097	-5.9	10.0	1.73	83.0	191	8
M 20/2	1720-3	29.00	-13.82	2004	33.2	6.0	3.30	78.8	208	9
M 20/2	1721-5	29.17	-13.08	3045	18.9	6.0	1.41	84.8	186	9
M 20/2	1728-3	29.83	-2.40	2887	23.8	2.0	0.30	94.9	229	7
M 20/2	1729-1	28.88	-1.00	4401	-0.1	0.6	0.08	93.6	211	6
M 34/3	3803-1	30.34	8.57	4173	3.1	0.8	0.16	90.0	199	10
M 34/3	3804-2	30.74	8.77	3882	7.8	0.7	0.12	92.2	184	10
M 34/3	3827-1	25.02	38.54	3842	-4.3	0.9	0.18	50.5	176	9
M 46/3	6330-1	46.15	57.56	3874	-13.1	No data	No data	No data	162	7

Table 1: Multiple core sample locations, depth (m), Deep water degree of $\Delta[CO_3^{2-}]$ (μmol kg^{-1}), Linear Sedimentation Rate (cm kyr^{-1}), TOC (Total Organic Caron) accumulation rate (g m^{-2} y^{-1}) and *Cibicidoides wuellerstorfi* B/Ca ratio (μmol mol^{-1}) at each sampling site.

2.2. X-ray Micro-CT Scanning

The XMCT system (ScanXmate-D160TSS105/11000, WhiteRabbit Corp., Tokyo, Japan) at the Japan Agency for Marine-Earth Science and Technology, Yokosuka, Japan, was used to obtain three-dimensional X-ray images of foraminiferal shells. The imaging was carried out with a high-resolution setting (X-ray focus spot diameter, 0.8 μm; X-ray tube voltage, 80 kV; detector array size, 2000 × 1336; 1500 projections/360°; 0.5 s/projection). After XMCT scanning, ConeCTexpress software (WhiteRabbit Corp., Tokyo, Japan) was used to convert the raw tomography data into segmented images of foraminifera shells. Image cross-sections were reconstructed from filtered back projections following the general principle of Feldkamp cone-beam reconstruction. The scanning and data processing methods followed a previous study [Iwasaki et al., 2015]. The CT number, indicating calcite density and visualizable porosity, was calculated based on the X-ray attenuation coefficient of each sample. We used Molcer Plus 3-D imaging software (WhiteRabbit Corp., Tokyo, Japan) to obtain isosurface images of the shells. Then, we evaluated the CT number histograms of each shell based on the 3-D tomography data.

2.3. Protocol of CT data processing for calculating CTDX

The CT scanning-based dissolution index (CTDX) of the planktic foraminiferal test employed in this study follows the same concept as the proxy of %Low-CT-number calcite volume previously suggested (Iwasaki et al., 2019, 2022). However, in this study, we modify the %Low-CT-number calcite volume proxy in a way that the resulting value is not dependent on the exact settings of the scanner, enabling applications using other X-ray micro-CT scanners, which had been modified to remove beam-hardening effects for assessing quantitative bulk density (i.e. submicron scale porosity) of organic carbonate. The protocol to calculate the value of CTDX from Serial Cross-Sectional Images of each specimen is shown in Figure 3. First, from the initial raw data (sequential sectional images) (Figure 3a), contaminants (e.g., detritus, fragments and other small foraminifera shells) stuck inside the test were removed by manual digital image processing (Figure 3b). After that, to segment shell material from other environments, we determined the lower threshold CT value by visual inspection of multiple specimens, ensuring only shell material is included. Under the process of segmentation, to facilitate a replicable smoothing of the shell surface and to make sure all voxels attached to the shell surface are included, we introduce a step where the six-neighboring voxels of a voxel located on the air-calcite boundary are retained. This is important to maintain voxels that partially contain shell material for the analysis. CT values in voxels retained after cleaning, segmentation, and thresholding were used to generate a CT histogram of the foraminiferal shell that could be used to calculate the dissolution index (Figure 3c). Previous studies [Iwasaki et al. 2019, 2022] suggested that the CT number histogram changes from monomodal to bimodal distribution with increasing dissolution. Based on this characteristic of change in the histogram shape with test dissolution, they proposed the relative volume of low-CT-number calcite to the volume of calcite in the whole shell (%Low-CT-number calcite volume) as a quantitative carbonate dissolution proxy for dissolution. Here we build on this approach but develop a new Dissolution Index (CTDX), which defines the threshold CT value independently of the scanner setting, using the shape of the CT value histogram. To this end, we first scaled the original CT number histogram by assigning 0 and 100 to the voxels with the lowest and highest CT values (Figure 3d). After that, we calculated the CTDX as the area ratio of the lower part of the histogram (X-axis: 0-50) to the whole histogram (X-axis: 0-100) (Figure 3e). Finally, we assigned a CTDX value to a sample as the average CTDX value of at least eight individual specimens. The minimum number

of shells needed to provide a representative estimate of the average preservation state of a given foraminifera species was determined by Iwasaki et al. (2022).

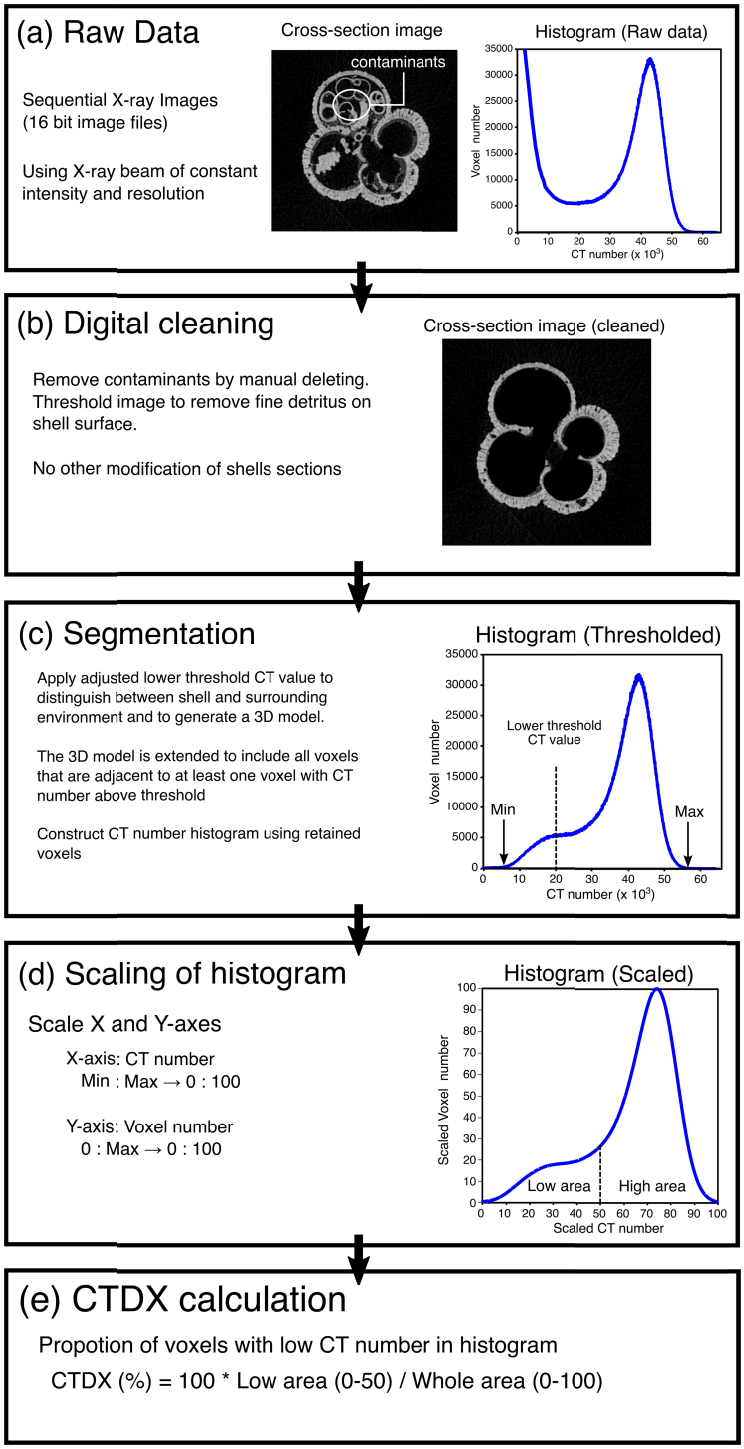

Figure 3. The protocol to calculate the foraminiferal shell dissolution index (CTDX) starts from raw sequential X-ray image data (a). (b) Contaminants in the shell sample are removed by manual deleting. (c) Apply threshold to distinguish between calcite material and surrounding

environment. Extract CT number histogram from cleaned and threshold 3D data. (d) Scaling X and Y-axes of CT number histogram. (e) Calculation of CTDX (%).

3 Results

3.1.Evaluating test dissolution by X-ray micro-CT scanning

The X-ray micro-CT scanning enables us to observe the internal structure of the foraminiferal shell and calcite density distribution in a single specimen's shell. The CT number histogram provides an objective and quantitative means to evaluate microscale calcite density distribution in each specimen. The Figure 4 shows the changes in the internal shell structure and CT number histogram of four species of planktic foraminifera in three seafloor sediment samples representing different locations and bottom water $\Delta[CO_3^{2-}]$ conditions. As expected, and in agreement with previous studies (Johnson et al., 2010, Iwasaki et al., 2019), we find a progression of shell dissolution with decreasing $\Delta[CO_3^{2-}]$. The dissolution first affects the septa among the juvenile chambers and then spreads to the inner layer of the chambers in the final whorl. With progressive dissolution, the CT number histograms show a shift from a unimodal distribution with a single, high CT number peak to a bimodal distribution, followed by a trend toward a unimodal density distribution with a peak at a low CT number. These are consistent with the results of previous studies (Iwasaki et al., 2015, 2019), suggesting that the shape of the CT number histogram, irrespective of the CT scanning settings, can be used to describe the preservation state of the foraminiferal shell.

Assuming that the shape of the CT number histogram, converted to the CTDX value as described above, quantify the degree of shell alteration due to selective dissolution (removal) of the most susceptible parts of the shell, the CTDX-based average state of shells of a given species of planktonic foraminifera should show a systematic relationship with deep-water chemistry. This is important, because the CTDX value is independent of the size and shape of the analyzed individual shells. It describes the portion of the shell that is affected by dissolution, irrespective of the analyzed calcite volume. In theory, the CTDX could even be applied to multiple species of foraminifera, but because the shell architectures among species vary significantly, we began by comparing the *G. bulloides* CTDX with that of three other species (*G. ruber, T. sacculifer*, and *G. inflata*) in the same sediment samples to also evaluate the inter-species variation in CTDX (Figure 5). The results shows that CTDX of *G. bulloides* significantly correlates with the other three species (*G. ruber*: $R^2 = 0.7$, *T. sacculifer*: $R^2 = 0.72$, *G. inflata*: $R^2 = 0.81$), suggesting that the CTDX of each of the species should be applicable as a dissolution proxy. However, the CTDX values among the species are offset, in particular for the relationship between CTDX of *G. bulloides, T. sacculifer* and *G. inflata*, the slopes of regression lines are relatively high (*T. sacculifer*: 1.69, *G. inflata*: 1.39). This implies that *T. sacculifer* and *G. inflata* are more sensitive to dissolution expressed by the CTDX index than *G. bulloides*.

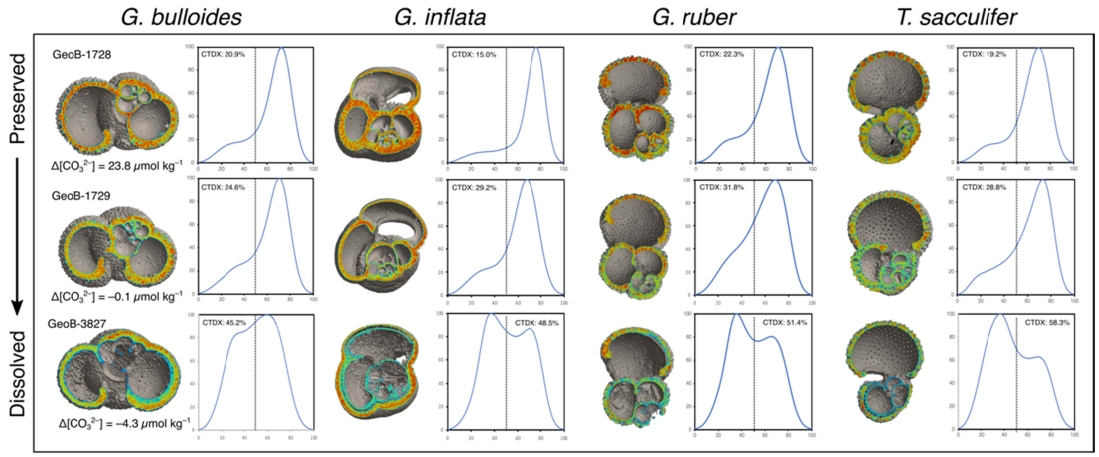

Figure 4. Changes in cross-sectional isosurface images and CT number histograms of four major species of planktonic foraminiferal shells (*G. bulloides, G. inflata, G. ruber* and *T. sacculifer*) with the progression of dissolution. Shells were obtained from three core top samples (GeoB-1728, 1729, and 3827). The condition of selected tests, which have CTDX similar to average of each sample set, are shown. $\Delta[CO_3^{2-}]$ at the nearest GLODAP stations at the core-top sample depths ranged from –4.3 to 23.8 μmol kg^{-1}. The dashed line in the CT number histograms shows the threshold (50) between low and high values.

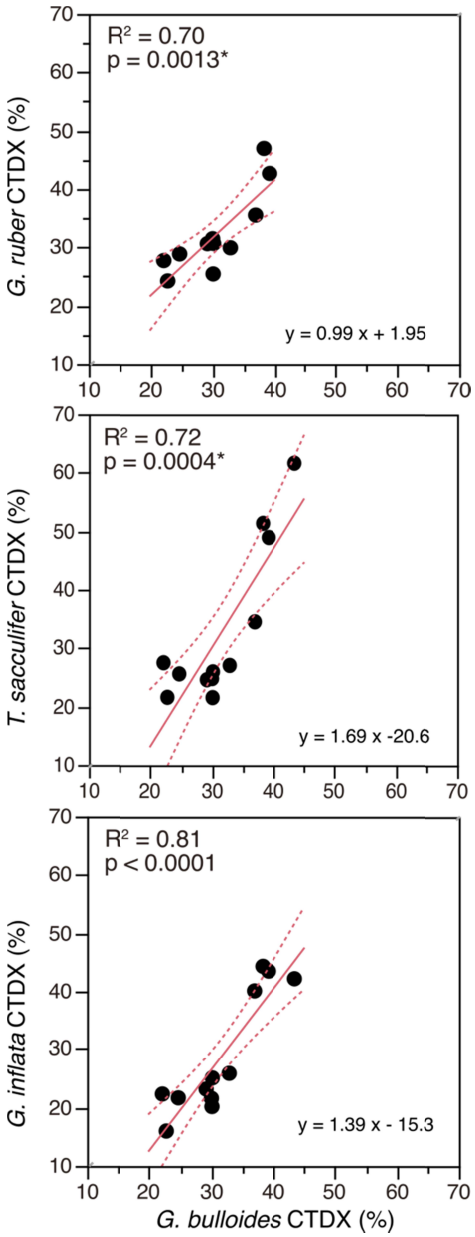

Figure 5. Inter species comparison of *G. bulloides* CTDX with other three species obtained from same core-top samples. The square of the correlation coefficient (R^2) and the type I error rate (*p*-value) are also shown.

3.2. Comparison between planktonic foraminiferal CTDX, bottom water $\Delta[CO_3^{2-}]$, MAR, and organic carbon flux

To assess the main controlling factors on foraminifera shell dissolution on the deep seafloor, we compared the planktonic foraminiferal shell CTDX values as a carbonate dissolution index, with three parameters: Bottom water $\Delta[CO_3^{2-}]$ representing ambient seawater corrosiveness, Linear Sedimentation Rate describing the exposure time of the shells on the seafloor, and Organic carbonate accumulation rate approximating supralysoclinal dissolution due to elevated porewater CO_2 from organic matter remineralization, for the 13 Atlantic samples where all parameters were available (Figure 6). First, we found a significant correlation between the

planktonic foraminiferal CTDX and the bottom water $\Delta[CO_3^{2-}]$ under the low $\Delta[CO_3^{2-}]$ condition (< 10 µmol kg^{-1}): *G. bulloides*; $R^2 = 0.87$, *G. inflata*; $R^2 = 0.85$, *G. ruber*; $R^2 = 0.77$, *T. sacculifer*; $R^2 = 0.80$ (Figure 6a). In contrast, the comparison between CTDX and sedimentation rate site did not show any support for the hypothesis that higher sedimentation rate facilitates better preservation of carbonate by faster burial (Figure 6b). These results suggest that the carbonate dissolution intensity in the South Atlantic is generally governed by ottom water $\Delta[CO_3^{2-}]$ under low $\Delta[CO_3^{2-}]$ condition (< 10 µmol kg^{-1}), not by sedimentation rate. Under high $\Delta[CO_3^{2-}]$ conditions (> 10 µmol kg^{-1}), high CTDX values are observed at two sites (GeoB 1720 and 1721), suggesting significant dissolution of carbonate, despite the supersaturated conditions for calcite in the ambient seawater. Here, a comparison with organic carbon accumulation rate (g cm^{-2} kyr^{-1}) reveals that the organic carbon inputs at both sites is more than three times higher than at the other sites (Figure 6c). These results indicate that organic carbon decomposition in the seafloor sediment may affect preservation of planktonic foraminifera shells even under supralysoclinal conditions (> 10 µmol kg^{-1}).

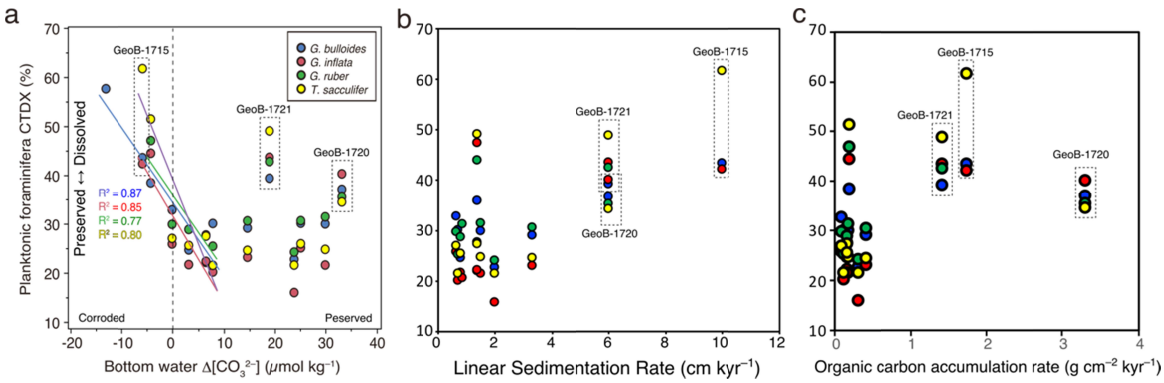

Figure 6. Investigation in controlling factor of foraminiferal shell dissolution intensity. (a) Bottom water $\Delta[CO_3^{2-}]$ (µmol kg^{-1}), (b) Liner Sedimentation Rate (cm kyr^{-1}), and (c) Organic carbon accumulation rate (g cm^{-2} kyr^{-1}) versus Planktonic foraminifera CTDX (%) at each sampling site. The data points at the sites locate in the Benguela upwelling system (GeoB-1715, 1720 and 1721) with high organic carbon accumulation rate are surrounded by dotted line.

3.3.Comparison with the proxy of benthic foraminiferal B/Ca ratio

To investigate the applicability of the CTDX as a deep seawater $\Delta[CO_3^{2-}]$ proxy, we next compared the CTDX values in the 13 South Atlantic samples with the B/Ca ratio of benthic foraminifera (*C. wuellerstorfi*) (Figure 7). The B/Ca ratio of benthic foraminifera (*C. wuellerstorfi*), a conventional quantitative proxy of deep seawater $\Delta[CO_3^{2-}]$, derived from the same sediment samples showed a weak correlation with the CTDX of each species: *G. bulloides*; $R^2 = 0.42$, $p = 0.0169$*, *G. inflata*; $R^2 = 0.24$, $p = 0.1034$, *G. ruber*; $R^2 = 0.27$, $p = 0.1034$, *T. sacculifer*; $R^2 = 0.28$, $p = 0.0960$ (Figure 7). The correlation has in all cases the expected sign (both proxies indicating more dissolution in the same samples), but the observation that the CTDX and B/Ca ratio correlation is not as pronounced as the correlation between CTDX and the bottom water $\Delta[CO_3^{2-}]$ is puzzling. Next, we focused on the *G. bulloides* CTDX, because this species was found at all sites, and showed the most significant correlation with the benthic foraminiferal B/Ca ratio among four species. The Figure 8 shows the relationship between two

proxies (*G. bulloides* CTDX and benthic foraminifera B/Ca ratio) and the bottom water $\Delta[CO_3^{2-}]$ under the lower deep seawater $\Delta[CO_3^{2-}]$ condition (< 10 µmol kg^{-1}). Based on this comparison, we identified the sites where either proxy is discrepant, and investigated the factors that may be responsible for the discrepancy in these two proxies. In this plot, the regression lines between *G. bulloides* CTDX and bottom water $\Delta[CO_3^{2-}]$ obtained from the results of this study and that between the benthic foraminiferal B/Ca ratio and bottom water $\Delta[CO_3^{2-}]$ obtained from the results of calibration using more than 200 core-top samples (Yu et al., 2013) were presented. The result shows that the benthic foraminiferal B/Ca ratio is at least 20 µmol mol^{-1} higher than the regression line at two sites: Site 1715 (Depth: 4097 m, bottom water $\Delta[CO_3^{2-}]$: –5.87 µmol kg^{-1}); Site 1729 (Depth: 4401 m, bottom water $\Delta[CO_3^{2-}]$: –0.10 µmol kg^{-1}). At those sites, the estimated value of bottom water $\Delta[CO_3^{2-}]$ derived from the benthic foraminiferal B/Ca ratio imply higher than observed $\Delta[CO_3^{2-}]$.

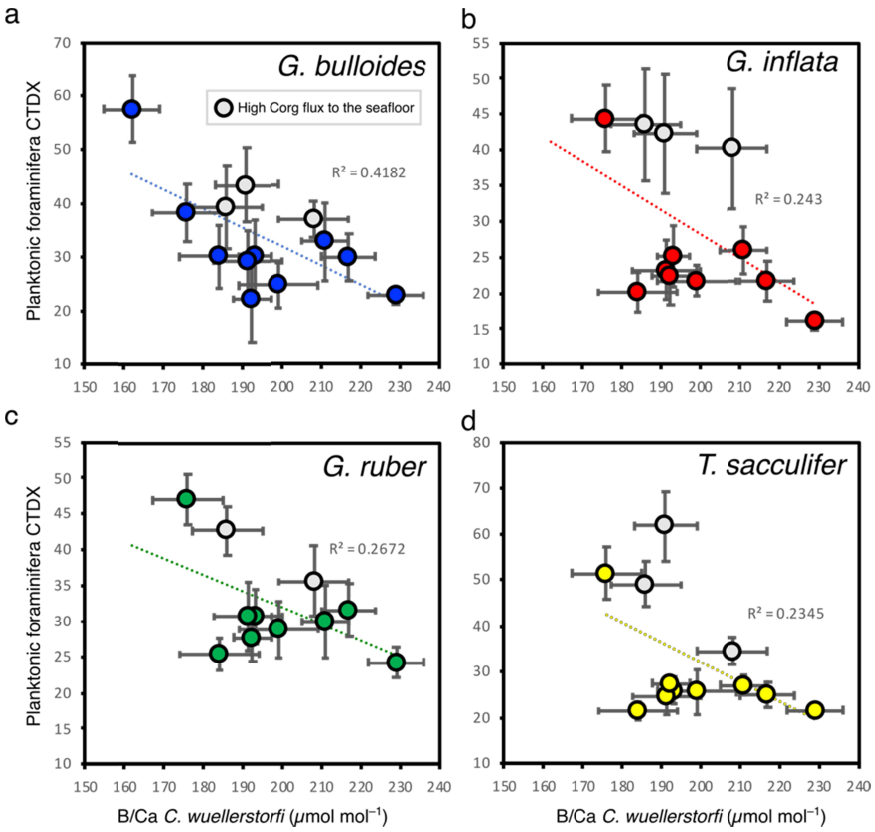

Figure 7. Relationship between planktonic foraminiferal CTDX of (a) *G. bulloides*, (b) *G. inflata*, (c) *G. ruber*, and (d) *T. sacculifer* and B/Ca ratio of *C. wuellerstorfi* (µmol mol^{-1}) in each core-top sample. The sampling sites located in the Benguela upwelling system with high organic carbon flux are shown by gray circle. The regression line and the square of the correlation coefficient (R^2) are also shown.

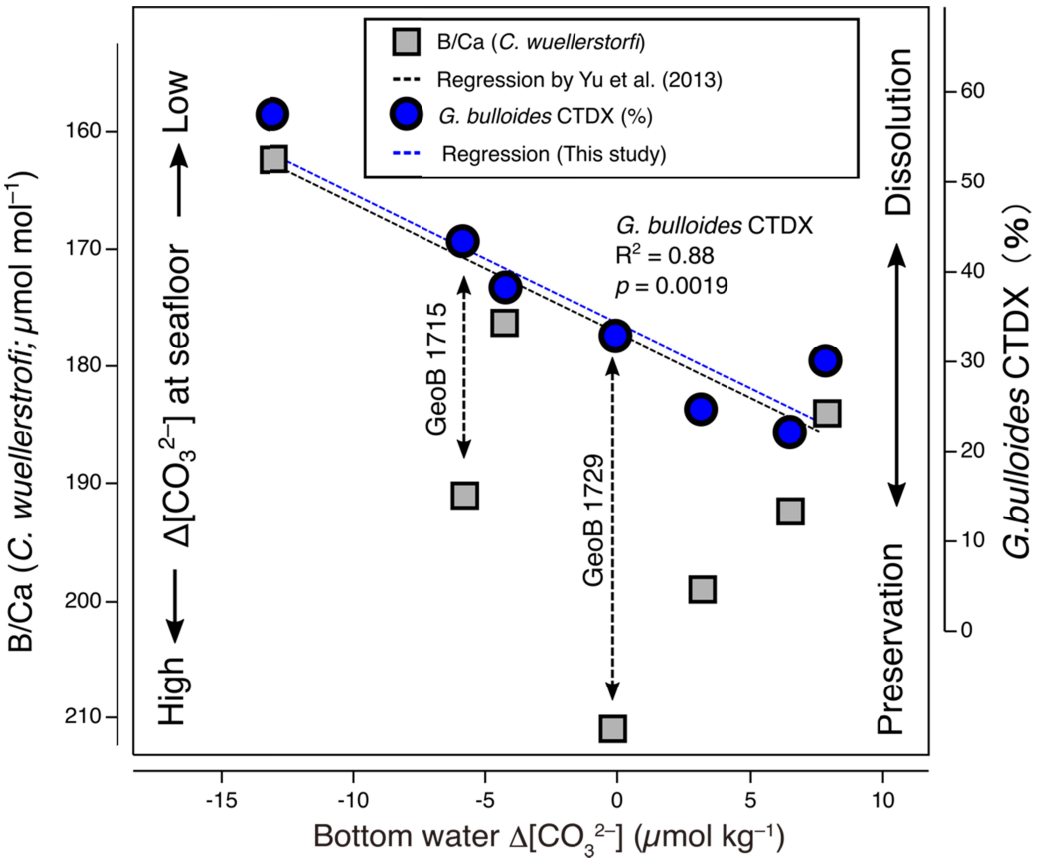

Figure 8. Comparison of the plots of *G. bulloides* CTDX and B/Ca ratio of *C. wuellerstorfi* against bottom seawater $\Delta[CO_3^{2-}]$ under the condition of low bottom seawater $\Delta[CO_3^{2-}]$ (< 10 µmol kg^{-1}). The B/Ca ratio of *C. wuellerstorfi* at the site GeoB-1715, 1729 and 3803 are relatively higher than *G. bulloides* CTDX.

3.4.Extended calibration between CTDX and deep water $\Delta[CO_3^{2-}]$

In addition to the 13 core top samples collected in the South Atlantic, we added the 16 core top samples collected in the Pacific Ocean to assess the behavior of the CTDX proxy under the condition of low deep seawater $\Delta[CO_3^{2-}]$ (< 10 µmol kg^{-1}) and to obtain an extended calibration equation between CTDX and deep seawater $\Delta[CO_3^{2-}]$ in the wider range of global ocean. The plot shows the relationship between the CTDX of three species of major planktic foraminiferal shell (*G. bulloides, G. ruber* and *T. sacculifer*) and deep water $\Delta[CO_3^{2-}]$ obtained from nearby bottle water sampling at each site (Figure 9). The sites at GeoB 1720 and 1721, with high organic material deposition, are excluded from the plot. The plot provides the relationship between CTDX and a wide range of deep seawater $\Delta[CO_3^{2-}]$ (–27 to 30 µmol kg^{-1}), and suggests that CTDX of each species significantly correlate with deep seawater $\Delta[CO_3^{2-}]$ between the range of –20 to 10 µmol kg^{-1}. The results of calibrations in each species are as follows:

G. bulloides: Deep seawater $\Delta[CO_3^{2-}] = -0.65 * CTDX + 24.8$ ($R^2 = 0.57$, N = 15)
G. ruber: Deep seawater $\Delta[CO_3^{2-}] = -0.56 * CTDX + 20.5$ ($R^2 = 0.88$, N = 12)
T. sacculifer: Deep seawater $\Delta[CO_3^{2-}] = -0.43 * CTDX + 15.3$ ($R^2 = 0.88$, N = 13)

These calibrations revealed that the CTDX of planktonic foraminifera are able to works as deep-water [CO_3^{2-}] proxy in the specific range of the deep seawater $\Delta[CO_3^{2-}]$ (–20 to 10 µmol kg^{-1}). However, the variation in the slope of regression line for each species indicated that the sensitivity of CTDX to dissolution varied among species. Based on the regression analysis, the uncertainties of the above regression equations are ±5.7 µmol kg^{-1} (*G. bulloides*, N = 15), ±2.8 µmol kg^{-1} (*G. ruber*, N = 12), and ±2.6 µmol kg^{-1} (*T. sacculifer*, N = 13). On the other hand, the CTDX shows stable values of around 25 and 60 under the high (> 10 µmol kg^{-1}) and low (< –20 µmol kg^{-1}) carbonate saturation state condition, respectively.

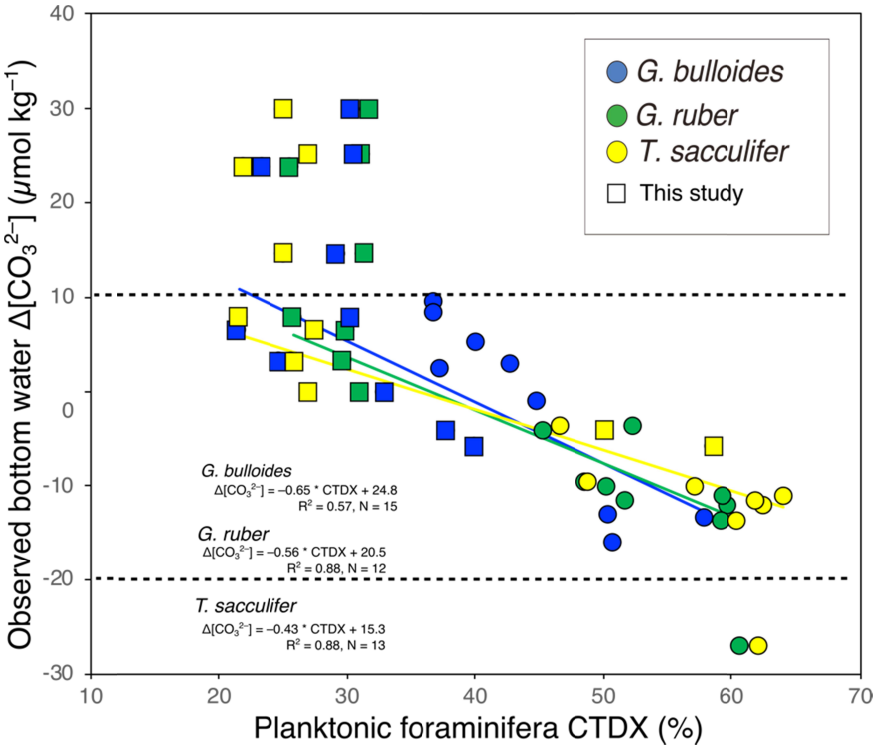

Figure 9. The CTDX of planktonic foraminifera (*G. bulloides, G. ruber* and *T. sacculifer*) in core top samples plotted against deep-water $\Delta[CO_3^{2-}]$. Core-top samples are obtained from this study and previous studies (Iwasaki et al., 2019 and 2022).

4 Discussion

4.1.Controlling factors of the planktonic foraminiferal CTDX

Dissolution of the planktonic foraminiferal shell is considered to occur mainly on deep seafloor under the control of ambient seawater $\Delta[CO_3^{2-}]$. At the same time, it can be affected by the variance in sedimentation rate and organic carbon respiration at the sediment surface [e.g., Berger et al., 1982, Milliman, 1993]. The direct comparisons between three numerical indexes derived from deep seafloor in this study (i.e., planktic foraminiferal CTDX, bottom water $\Delta[CO_3^{2-}]$, the sedimentation rate, and the organic carbon accumulation rate at each site) provided the critical information to identify the controlling factor of carbonate dissolution at the deep seafloor. First, the significant correlation between the proxy of CTDX and bottom water $\Delta[CO_3^{2-}$

] proves that dissolution of the planktic foraminiferal shell is undoubtedly controlled by bottom water $\Delta[CO_3^{2-}]$ in the most sites under the lower condition of bottom water $\Delta[CO_3^{2-}]$ (< 10 µmol kg^{-1}). Second, the sedimentation rate is not correlated with the planktic foraminiferal CTDX. This result suggests that the variance in sedimentation rate, which corresponds to approx. 5-to-10-fold difference in sedimentation rate does not significantly impact the carbonate dissolution variance at the deep seafloor. Third, the CTDX showed significantly higher values at two data sites (GeoB-1720 and 1721) than at the other data points under the condition of higher deep seawater $\Delta[CO_3^{2-}]$ (> 10 µmol kg^{-1}), which implies the exceeded carbonate dissolution under the supersaturated condition. These two sites are located at the Benguela Upwelling System in the eastern South Atlantic, one of the significant continental margins upwelling systems and belongs to the high productivity area of the ocean [Berger, 1989]. Previous research in the Benguela Upwelling System suggested that carbonate dissolution occurs at 400-1600 m above the lysocline by the above process (Vobers and Hinrich, 2002), induced by the release of CO_2 due to the oxidation of organic material within the sediment (Emerson and Bender, 1981; Archer, 1991; Jahnke et al., 1994). In addition, the other potential factor is that the porous shell, possibly response to rapid chamber formation, resulting in the formation of shells that are prone to dissolution. Culture studies have shown that the chamber formation rate increases under the food abundant condition as like as upwelling region (Bé et al., 2009), and such high chamber formation rate could provide the porous shell formation (Berger, 1970). In either case, we consider that the observed dissolution of planktonic foraminifera shells in the sediments derived from the Benguela Upwelling System in this study is not controlled by deep seawater $\Delta[CO_3^{2-}]$, but was probably brought yb other factors such as decomposition of organic material occurring above the regional lysocline and ontogenetic growth condition at sea surface.

On the other hand, the relationship between benthic foraminiferal B/Ca ratio and deep-water $\Delta[CO_3^{2-}]$ did not show any unusual values at the sites from the Benguela Upwelling System, suggesting that the organic material decomposition does not have notable impact on benthic foraminiferal B/Ca ratio. We suppose that the reduction in seawater $\Delta[CO_3^{2-}]$, caused by organic material decomposition, has a more substantial influence on the dissolution of the planktonic foraminiferal test than the reduction in the B/Ca ratio of the benthic foraminiferal test. The mechanism to explain these results is to hypothesize that the decrease in seawater $\Delta[CO_3^{2-}]$ due to organic material decomposition occurs mainly inside the sediment or aggregates of organic material like marine snow or fecal pellets. Such organic material oxidization affects planktonic foraminifera shells co-deposited with such aggregates, but, it does not significantly affect the seafloor surface or outside of the aggregates (i.e., the habitat area of benthic foraminifera). These findings suggests that the planktonic foraminiferal CTDX is not a suitable proxy at sites with high organic material deposition like upwelling system. The benthic foraminiferal B/Ca ratio is rather appropriate for use in such sample sites.

4.2. Deep seawater $[CO_3^{2-}]$ proxies: The characteristics of CTDX and B/Ca proxy

In this study, the characteristics of CTDX proxy were determined by measuring the dissolution intensity of four species of planktic foraminifera and comparing the several parameters derived from seafloor sediment samples in the South Atlantic. First, the results of inter-species comparisons (Figure 5) showed that the CTDX varies among the species, suggesting that species-specific application is required for accurate reconstruction. Nevertheless, our results suggested that the CTDX of all species are applicable as shell dissolution proxy. This

467 indicates that multiple species of planktonic foraminifera are applicable as deep-water [CO_3^{2-}]
468 proxy by establishing proxy calibration for each species. This is one of the essential advantages
469 of using CTDX over conventional proxies based on the B/Ca ratio of benthic foraminifera.
470 Therefore, it enables us to apply this new proxy to the foraminifera poor sediment cores, where it
471 is challenging to collect single species continuously. It also allows us to compare the
472 reconstructed data between sites from different locations with different planktic locations
473 foraminiferal species compositions.

474 Second, the relationship between the CTDX and the deep seawater $\Delta[CO_3^{2-}]$ suggested
475 that the CTDX significantly correlated with deep seawater $\Delta[CO_3^{2-}]$ only under the low deep
476 seawater $\Delta[CO_3^{2-}]$ condition (< 10 µmol kg^{-1}) (Figure 6, and Figure 9). However, under the
477 high deep seawater $\Delta[CO_3^{2-}]$ condition (> 10 µmol kg^{-1}), the values of planktic
478 foraminiferal CTDX were almost constant. Similar results were also represented by the
479 comparison between shell dissolution proxy and deep seawater $\Delta[CO_3^{2-}]$, suggesting the
480 saturation of shell dissolution proxy at the sites of high deep seawater $\Delta[CO_3^{2-}]$ (> 10
481 µmol/kg) [Johnstone et al., 2010]. Furthermore, under the extremely low deep seawater
482 $\Delta[CO_3^{2-}]$ condition (< –20 µmol kg^{-1}), the CTDX seems to saturate around the values of 60
483 (Figure 9). This implies that planktonic foraminiferal shells which appear intact (i.e., which
484 are not broken or fragmented and retain the outermost chamber) show maximum CTDX
485 values of around 60. It is likely that with further progressing dissolution the shells lose
486 structural integrity, break into fragments and would fall outside of the sample selection for
487 CT scanning. From the above, we conclude that the CTDX proxy works effectively under
488 deep seawater $\Delta[CO_3^{2-}]$ lower than 10 µmol kg^{-1} and higher than –20 µmol kg^{-1}.
489 Alternatively, we suppose that the analysis of fragmented individual is useful for applying
490 CTDX under the significantly low deep seawater $\Delta[CO_3^{2-}]$ condition (< –20 µmol kg^{-1}).

491 We also evaluated the accuracy of the deep seawater [CO_3^{2-}] reconstruction by each
492 proxy. Under the low deep seawater $\Delta[CO_3^{2-}]$ (< 10 µmol/kg) condition, the proxy of CTDX
493 showed a correlation with the deep seawater $\Delta[CO_3^{2-}]$ and the conventional proxy of benthic
494 foraminiferal B/Ca ratio (Figure 7). These results support our interpretation that the proxy of
495 CTDX can serve as an indicator of deep seawater $\Delta[CO_3^{2-}]$. Nevertheless, comparing these two
496 proxies, we found two peculiar sites (Sites GeoB-1715 and 1729) where the CTDX and B/Ca
497 ratio values deviate (Figure 8). The sediment samples at these two sites are rich in carbonate (>
498 80%), and the proxy of CTDX shows the occurrence of carbonate dissolution and relatively high
499 values of benthic foraminiferal B/Ca ratio than general estimation. We speculate that the process
500 of carbonate compensation in surface sediment may have raised [CO_3^{2-}] in the porewater and
501 contributed to the higher values of the benthic foraminiferal B/Ca ratio in a way similar to the
502 speculated protective effect of aragonite dissolution on carbonate preservation described by
503 Sulpice et al. (2022). To evaluate this speculation, we investigated the difference in total
504 alkalinity of porewater in the sediment surface (upper 5 cm) and the overlying bottom water
505 (Hensen et al., 2003a-d). The total alkalinity is a valuable indicator that relates to the seawater
506 [CO_3^{2-}] and is controlled by the carbonate dissolution in the sediment, which enables us to
507 presume the geochemical process in the sediment surface. The profiles of chemical parameters at
508 Site GeoB-1715 and 1729 showed that the total alkalinity in the pore water (average of the upper
509 5 cm) is more than 200 µmol kg^{-1} higher than in overlying bottom water as follows: GeoB-1715
510 (bottom water: 2354 µmol kg^{-1}, porewater average: 2583 µmol kg^{-1}) and GeoB-1729 (bottom
511 water: 2359 µmol kg^{-1}, porewater average: 2653 µmol kg^{-1}). In contrast, at Site GeoB-3804 and
512 3827 with appropriate benthic foraminiferal B/Ca ratio for the general estimation, the difference

in the total alkalinity between pore water and overlying bottom water is relatively small as follows: GeoB-3804 (bottom water: 2348 μmol kg^{-1}, porewater average: 2458 μmol kg^{-1}) and GeoB-3827 (bottom water: 2342 μmol kg^{-1}, porewater average: 2275 μmol kg^{-1}). These results imply that carbonate dissolution at the sediment surface discharges carbonate ions and raises the porewater's total alkalinity, altering the calcification condition for benthic foraminifera. From the above, we consider that the strong carbonate dissolution in the carbonate-rich sediment is one of the principles controlling factors of the benthic foraminiferal B/Ca ratio.

5 Conclusions

The assessments in planktic foraminiferal shell dissolution intensity, represented by CTDX, were directly compared with the data of B/Ca in benthic foraminifera in the same sample and the other proxies of conditions at each site (deep-water $\Delta[CO_3^{2-}]$, sedimentation rate, and Organic carbon accumulation rate). In addition, inter-species variation in CTDX of four species of planktic foraminifera were assessed. Our results proved that CTDX of each planktic foraminifera is generally controlled by deep-water $\Delta[CO_3^{2-}]$ variation like a conventional proxy of benthic foraminiferal B/Ca ratio. We suggested that four species (*G. bulloides, G. inflata, G. ruber*, and *T. sacculifer*) of planktonic foraminiferal CTDX are applicable as a quantitative proxy for carbonate dissolution intensity, while we recommend species-specific use of CTDX for accurate reconstruction because there is slight difference in sensitivity to dissolution. On the other hand, the effect of variation in sedimentation rate is not a significant factor in carbonate dissolution in the sediment surface if the difference in sedimentation rate is 5-to-10-fold difference or less. Based on the above results, we concluded that the proxy of planktic foraminiferal CTDX is applicable as a quantitative deep-water $[CO_3^{2-}]$ proxy as well as a conventional proxy of benthic foraminiferal B/Ca ratio. Nevertheless, there are several caveats in the application of each proxy. First, the proxy of CTDX is useful under the specific condition of deep-water $\Delta[CO_3^{2-}]$ between –20 to 10 μmol kg^{-1}, suggesting that the CTDX has a detection limit range of deep-water $[CO_3^{2-}]$. Therefore, we should exclude the seafloor sediment sample obtained from high deep-water $\Delta[CO_3^{2-}]$ condition (> 10 μmol kg^{-1}) in the process of establishing the calibration equation, and we have to note that this proxy is not reliable for reconstructing the higher deep-water $\Delta[CO_3^{2-}]$ in the application of CTDX into sediment core samples. Second, we also observed the excessive dissolution of planktic foraminifera in the supersaturated condition for calcite, which seems to be caused by the intensive input of organic material into seafloor sediment. Therefore, we consider that we should refrain from applying the CTDX proxy to the sediment sample located in the upwelling system where organic material input from the sea surface is exceptionally high. Third, we revealed that carbonate compensation, which occurs in carbonate-rich and carbonate dissolution affected sediment samples, may alter the benthic foraminiferal B/Ca ratio higher during their calcification, which may contribute to uncertainty of deep-water $[CO_3^{2-}]$ reconstruction by benthic foraminiferal B/Ca ratio.

Based on the suggested characteristics of CTDX, we provided the calibration formula between three species planktic foraminiferal (*G. bulloides, G. ruber* and *T. sacculifer*) CTDX and deep seawater $\Delta[CO_3^{2-}]$ using a number (N = 22) of seafloor sediment samples. Although the number of sediment samples and the distribution range of samples are inferior to the conventional proxy of benthic foraminiferal B/Ca ratio, our calibration showed that the proxy of CTDX works as well as the B/Ca proxy for deep seawater $[CO_3^{2-}]$ reconstruction under the suitable conditions. This proxy may help to fill the blank of paleo-deep-water $[CO_3^{2-}]$ data, in

558 particular, in the mid-high latitude of the North Pacific, where benthic foraminiferal B/Ca ratio
559 data are insufficient.
560
561

562 **Acknowledgments**

563 This study used samples that were collected during cruises M12/1, M20/2 and M34/3 by R/V
564 METEOR. The data reported in this paper are available in Supplemental Information. This study
565 was technically and financially supported by the Japan Agency for Marine-Earth Science and
566 Technology and the Cluster of Excellence "The Ocean Floor—Earth's Uncharted Interface"
567 funded by the German Research Foundation (DFG).
568

569

570 **Open Research**

571 The data used in this study will be available in PANGAEA (https://www.pangaea.de/).

572

573 **References**

574 Allen, K. A., E. L. Sikes, B. Hönisch, A. C. Elmore, T. P. Guilderson, Y. Rosenthal, and R. F.
575 Anderson (2015), Southwest Pacific deep water carbonate chemistry linked to high southern
576 latitude climate and atmospheric CO_2 during the Last Glacial Termination, *Quat. Sci. Rev.*, *122*,
577 180–191. doi:10.1016/j.quascirev.2015.05.007.
578
579 Allen, K. A., E. L. Sikes, R. F. Anderson, and Y. Rosenthal (2020), Rapid Loss of CO_2 From the
580 South Pacific Ocean During the Last Glacial Termination, *Paleoceanogr. Paleoclimatology*,
581 *35*(2), 1–13. doi:10.1029/2019PA003766.
582
583 Archer, D. E. (1991), Equatorial Pacific calcite preservation cycles: production or dissolution?
584 Paleoceanography, 6(5), 561–571.
585
586 Barker, S., and H. Elderfield (2002), Foraminiferal calcification response to glacial-interglacial
587 changes in atmospheric CO2., *Science*, 297, 833–836, doi:10.1126/science.1072815.
588
589 Barnola, J. M., D. Raynaud, Y. S. Korotkevicht, and C. Lorius (1987), Vostok ice core provides
590 160,000-year record of atmospheric CO_2, *Nat. Geosci.*, *329*, 408.
591
592
593 Bé, A.W.H., D.A. Caron, O.R. Anderson (1981), Effects of feeding frequency on life processes
594 of the planktonic foraminifer *Globigerinoides sacculifer* in laboratory culture, *Journal of the*

Marine Biological Association of the United Kingdom, 61, 257-277.

Berger, W. H. (1970), Diversity of Planktonic Foraminifera in Deep-Sea Sediments, *Science (80-.).*, *168*(3937), 1345–1347, doi:10.1126/science.168.3937.1345.

Berger, W. H., F. L. Parker, and L. Jolla (1982), Foraminifera on the deep-sea floor: lysocline and dissolution rate, *Oceanol. Acta*, *5*(2), 249–258.

Berger, W. (1989), Global maps of ocean productivity, in Productivity of the Ocean: Present and Past, edited by W. H. Berger, V. S. Smetacek, and G. Wefer, pp. 429–455, John Wiley, New York

Bleil, U. (2001), Report and preliminary results of Meteor Cruise M 46/3, Montevideo - Mar del Plata, 04.01-07.02.2000., Berichte, Fachbereich Geowissenschaften, Univ. Bremen, 172.

Broecker, W. S., and E. Clark (2001), Glacial-to-Holocene redistribution of carbonate ion in the deep sea., *Science*, 294, 2152–2155, doi:10.1126/science.1064171.

Brown, R. E., L. D. Anderson, E. Thomas, and J. C. Zachos (2011), A core-top calibration of B/Ca in the benthic foraminifers Nuttallides umbonifera and Oridorsalis umbonatus: A proxy for Cenozoic bottom water carbonate saturation, *Earth Planet. Sci. Lett.*, *310*(3–4), 360–368. doi:10.1016/j.epsl.2011.08.023.

Brown, S. J., and H. Elderfield (1996), Variations in Mg/Ca and Sr/Ca ratios of planktonic foraminifera caused by postdepositional dissolution: Evidence of shallow Mg-dependent dissolution, , 11(5), 543–551.

Emerson, S. and M. Bender (1981), Carbon fluxes at the sediment-water interface of the deep-sea: calcium carbonate preservation, Journal of Marine Research, 39, 139–162, 1981.

Geslin, E., P. Heinz, F. Jorissen, and C. Hemleben (2004), Migratory responses of deep-sea benthic foraminifera to variable oxygen conditions: Laboratory investigations, Mar. Micropaleontol., 53(3–4), 227–243, doi:10.1016/j.marmicro.2004.05.010.

Gooday, A. J. (2003), Benthic foraminifera (protista) as tools in deep-water palaeoceanography: Environmental influences on faunal characteristics, *Adv. Mar. Biol.*, *46*, 1–90.

Hales, B. (2003), Respiration, dissolution, and the lysocline, *Paleoceanography*, *18*(4), 1–14, doi:10.1029/2003PA000915.

Hales, B., and S. Emerson (1996), Calcite dissolution in sediments of the Ontong-Java Plateau: In situ measurements of pore water O_2 and pH, *Global Biogeochem. Cycles*, *10*(3), 527–541.

Hensen, Christian; Zabel, Matthias (2003a): Geochemistry of porewater in sediment core GeoB1715-3. PANGAEA, https://doi.org/10.1594/PANGAEA.105409

Hensen, Christian; Zabel, Matthias (2003b): Geochemistry of porewater in sediment core GeoB1729-2. PANGAEA, https://doi.org/10.1594/PANGAEA.105421

Hensen, Christian; Kasten, Sabine (2003c): Geochemistry of porewater in sediment core GeoB3804-2. PANGAEA, https://doi.org/10.1594/PANGAEA.105848

Hensen, Christian; Kasten, Sabine (2003d): Geochemistry of porewater in sediment core GeoB3827-1. PANGAEA, https://doi.org/10.1594/PANGAEA.105893

Hemming, N. G., and G. N. Hanson (1992), Boron isotopic composition and concentration in modern marine carbonates, *Geochim. Cosmochim. Acta*, *56*(1), 537–543. https://doi:10.1016/0016-7037(92)90151-8.

Iwasaki, S., K. Kimoto, O. Sasaki, H. Kano, M. C. Honda, and Y. Okazaki (2015), Observation of the dissolution process of Globigerina bulloides tests (planktic foraminifera) by X-ray microcomputed tomography, *Paleoceanography*, *30*(4), 317–331, doi:10.1002/2014PA002639.

Iwasaki, S., K. Kimoto, O. Sasaki, H. Kano, and H. Uchida (2019), Sensitivity of planktic foraminiferal test bulk density to ocean acidification, *Sci. Rep.*, *9*, 1–9, doi:10.1038/s41598-019-46041-x.

Iwasaki, S., L. Lembke-jene, K. Nagashima, H. W. Arz, N. Harada, K. Kimoto, and F. Lamy (2022), Evidence for late-glacial oceanic carbon redistribution and discharge from the Paci fi c Southern Ocean, *Nat. Commun.*, *13*(6250), doi:10.1038/s41467-022-33753-4.

Jahnke, R. A., D. B. Craven, and J.-F. Gaillard (1994), The influence of organic matter diagenesis on $CaCO_3$ dissolution at the deep-sea floor, Geochim. Cosmochim. Acta, 58(13), 2799–2809.

Johnstone, H. J. H., M. Schulz, S. Barker, and H. Elderfield (2010), Inside story: An X-ray computed tomography method for assessing dissolution in the tests of planktonic foraminifera, *Mar. Micropaleontol.*, *77*(1–2), 58–70, doi:10.1016/j.marmicro.2010.07.004.

Key, R. M., A. Kozyr, C. L. Sabine, K. Lee, R. Wanninkhof, J. L. Bullister, R. A. Feely, F. J. Millero, C. Mordy, and T. H. Peng (2004), A global ocean carbon climatology: Results from Global Data Analysis Project (GLODAP), Global Biogeochem. Cycles, 18, 1–23, doi:10.1029/2004GB002247.

Kitazato, H. et al. (2000), Seasonal phytodetritus deposition and responses of bathyal benthic foraminiferal populations in Sagami Bay, Japan: Preliminary results from "Project Sagami 1996-1999," *Mar. Micropaleontol.*, *40*(3), 135–149, doi:10.1016/S0377-8398(00)00036-0.

Kucera, M. (2007). Chapter Six: Planktonic foraminifera as tracers of past oceanic environments. Developments in Marine Geology, 1, 213–262.

Lohmann, G. P. (1995), A model for variation in the chemistry of planktonic foraminifera due to secondary calcification and selective dissolution, Paleoceanography, 10(3), 445–457.

Marshall, B. J., R. C. Thunell, M. J. Henehan, Y. Astor, and K. E. Wejnert (2013), Planktonic foraminiferal area density as a proxy for carbonate ion concentration: A calibration study using the Cariaco Basin ocean time series, *Paleoceanography*, *28*(2), 363–376, doi:10.1002/palo.20034.

Milliman, J. D. (1993), Production and accumulation of calcium carbonate in the ocean: Budget of a nonsteady state, *Global Biogeochem. Cycles*, *7*(4), 927–957, doi:10.1038/181669b0.

Mollenhauer, G et al. (2004): Organic carbon accumulation in the South Atlantic Ocean: its modern, mid-Holocene and last glacial distribution. Global and Planetary Change, 40(3-4), 249-266, https://doi.org/10.1016/j.gloplacha.2003.08.002

Müller, Peter J (2004): Carbon and nitrogen data of sediment core GeoB1715-1. Department of Geosciences, Bremen University, PANGAEA, https://doi.org/10.1594/PANGAEA.143542

Morard, R. et al. (2019), Genetic and morphological divergence in the warm-water planktonic foraminifera genus Globigerinoides, *PLoS One*, *14*(12), 1–30, doi:10.1371/journal.pone.0225246.

Peterson, L. C., and W. L. Prell (1985), Carbonate dissolution in recent sediments of the eastern Equatorial Indian Ocean: preservation patterns and carbonate loss above the lysocline, *Mar. Geol.*, *64*, 259–290.

Petit, J. R. et al. (1999), Climate and atmospheric history of the past 420,000 years from the Vostok ice core, Antarctica, *Nature*, *399*(6735), 429–436. https://doi:10.1038/20859.

Rae, J. W. B., G. L. Foster, D. N. Schmidt, and T. Elliott (2011), Boron isotopes and B/Ca in benthic foraminifera: Proxies for the deep ocean carbonate system, *Earth Planet. Sci. Lett.*, *302*(3–4), 403–413. https://doi:10.1016/j.epsl.2010.12.034.

Raitzsch, M., E. C. Hathorne, H. Kuhnert, J. Groeneveld, and T. Bickert (2011), Modern and late pleistocene B/Ca ratios of the benthic foraminifer Planulina wuellerstorfidetermined with laser ablation ICP-MS, *Geology*, *39*(11), 1039–1042. doi:10.1130/G32009.1.

Schiebel, R. (2002), Planktic foraminiferal sedimentation and the marine calcite budget, *Global Biogeochem. Cycles*, *16*(4), 3-1-3–21. doi:10.1029/2001gb001459.

Schulz, HD and et al(1992)Bericht und erste Ergebnisse über die Meteor-Fahrt M20/2, Abidjan-Dakar, 27.12.1991-3.2.1992.Berichte aus dem Fachbereich Geowissenschaften der Universität Bremen, 025. Department of Geosciences, Bremen University. urn:nbn:de:gbv:46-ep000101614

Sigman, D. M., and E. A. Boyle (2000), Glacial/interglacial variations in atmospheric carbon dioxide, *Nature*, *407*(19), 859–869. https://doi.org/10.1038/35038000.

Sulpis, O., P. Agrawal, M. Wolthers, G. Munhoven, M. Walker, and J. J. Middelburg (2022), Aragonite dissolution protects calcite at the seafloor, *Nat. Commun.*, *13*(1), 1–8, doi:10.1038/s41467-022-28711-z.

Volbers, A. N., and R. Henrich (2002), Late Quaternary variations in calcium carbonate preservation of deep-sea sediments in the northern Cape Basin: results from a multiproxy approach, Mar. Geol., 180(1–4), 203–220, doi:10.1016/S0025-3227(01)00214-6.

Wefer, G and et al (1990), Bericht über die Meteor-Fahrt M12/1, Kapstadt-Funchal, 13.3.-14.4.1990.Berichte aus dem Fachbereich Geowissenschaften der Universität Bremen, 011. Department of Geosciences, Bremen University. urn:nbn:de:gbv:46-ep000101534

Wefer, G. (1996), Report and preliminary results of METEOR-Cruise M34/3, Walvis Bay - Recife, 21.2.-17.3.1996., Berichte, Fachbereich Geowissenschaften, Univ. Bremen, 79.

Yu, J., and H. Elderfield (2007), Benthic foraminiferal B/Ca ratios reflect deep water carbonate saturation state, *Earth Planet. Sci. Lett.*, *258*(1–2), 73–86. https:/doi:10.1016/j.epsl.2007.03.025.

Yu, J., R. F. Anderson, Z. Jin, J. W. B. Rae, B. N. Opdyke, and S. M. Eggins (2013), Responses of the deep ocean carbonate system to carbon reorganization during the Last Glacial-interglacial cycle, *Quat. Sci. Rev.*, *76*, 39–52. doi:10.1016/j.quascirev.2013.06.020.

Yu, J. et al. (2016), Sequestration of carbon in the deep Atlantic during the last glaciation, *Nat. Geosci.*, *9*(4), 319–324. doi:10.1038/ngeo2657.

Yu, J. et al. (2020), Last glacial atmospheric CO2 decline due to widespread Pacific deep-water expansion, Nat. Geosci., 13, 628–633, doi:10.1038/s41561-020-0610-5.

Figure chaptions

Figure 1. The locations of multiple corer samples in the South Atlantic used in this study. The section along the yellow line is showing the spatial distribution of the degree of carbonate saturation ($\Delta[CO_3^{2-}]$) in the study area.

Figure 2. B/Ca ratio in shells of the benthic foraminifera *Cibicidoides wuellerstorfi* in core top samples plotted against deep-water $\Delta[CO_3^{2-}]$. The data of B/Ca ratio of benthic foraminifera in the core-top sample used in this study are shown by blue squares. Data are derived from Rae et al. (2011), Raitzch et al. (2011), and Yu and Elderfield (2007).

Figure 3. Protocol to calculate the foraminiferal shell dissolution index (CTDX) start from raw sequential X-ray image data (a). (b) Contaminants in the shell sample are removed by manual deleting. (c) Apply threshold to distinguish between calcite material and surrounding environment. Extract CT number histogram from cleaned and threshold 3D data. (d) Scaling X and Y-axes of CT number histogram. (e) Calculation of CTDX (%).

Figure 4. Changes in cross-sectional isosurface images and CT number histograms of four major species of planktonic foraminiferal shells (*G. bulloides, G. inflata, G. ruber* and *T. sacculifer*) with the progression of dissolution. Shells were obtained from three core top samples (GeoB-1728, 1729, and 3827). The condition of selected tests, which have CTDX similar to average of each sample set, are shown. $\Delta[CO_3^{2-}]$ at the nearest GLODAP stations at the core-top sample depths ranged from –4.3 to 23.8 μmol kg^{-1}. The dashed line in the CT number histograms shows the threshold (50) between low and high values.

Figure 5. Inter species comparison of *G. bulloides* CTDX with other three species obtained from same core-top samples. The square of the correlation coefficient (R^2) and the type I error rate (*p*-value) are also shown.

Figure 6. Investigation in controlling factor of foraminiferal shell dissolution intensity. (a) Bottom water $\Delta[CO_3^{2-}]$ (μmol kg^{-1}), (b) Liner Sedimentation Rate (cm kyr^{-1}), and (c) Organic carbon accumulation rate (g cm^{-2} kyr^{-1}) versus Planktonic foraminifera CTDX (%) at each sampling site. The data points at the sites locate in the Benguela upwelling system (GeoB-1715, 1720 and 1721) with high organic carbon accumulation rate are surrounded by dotted line.

Figure 7. Relationship between planktonic foraminiferal CTDX of (a) *G. bulloides*, (b) *G. inflata*, (c) *G. ruber*, and (d) *T. sacculifer* and B/Ca ratio of *C. wuellerstorfi* (μmol mol^{-1}) in each core-top sample. The sampling sites located in the Benguela upwelling system with high organic carbon flux are shown by gray circle. The regression line and the square of the correlation coefficient (R^2) are also shown.

Figure 8. Comparison of the plots of *G. bulloides* CTDX and B/Ca ratio of *C. wuellerstorfi* against bottom seawater $\Delta[CO_3^{2-}]$ under the condition of low bottom seawater $\Delta[CO_3^{2-}]$ (< 10 μmol kg^{-1}). The B/Ca ratio of *C. wuellerstorfi* at the site GeoB-1715, 1729 and 3803 are relatively higher than *G. bulloides* CTDX.

Figure 9. The CTDX of planktonic foraminifera (*G. bulloides, G. ruber* and *T. sacculifer*) in core top samples plotted against deep-water $\Delta[CO_3^{2-}]$. Core-top samples are obtained from this study and previous studies (Iwasaki et al., 2019 and 2022).

Table 1. Multiple core sample locations, depth (m), Deep water degree of $\Delta[CO_3^{2-}]$ (μmol kg^{-1}), Linear Sedimentation Rate (cm kyr^{-1}), TOC (Total Organic Caron) accumulation rate (g m^{-2} y^{-1}) and *Cibicidoides wuellerstorfi* B/Ca ratio (μmol mol^{-1}) at each sampling site.